Letter

Chiral spin spiral in synthetic antiferromagnets probed by circular dichroism in x-ray resonant magnetic scattering

Cyril Léveillé,[1] Samuel Flewett,[2] Erick Burgos-Parra,[1,3] Yanis Sassi,[3] William Legrand,[3] Fernando Ajejas,[3] Vincent Cros,[3] Nicolas Reyren,[3] and Nicolas Jaouen[1]

[1]*Synchrotron SOLEIL, L'Orme des Merisiers, Saint-Aubin, Boîte Postale 48, 91192 Gif-sur-Yvette Cedex, France*
[2]*Instituto de Fisica, Pontificia Universidad Católica de Valparaíso, Avenida Universidad 330, Valparaíso, Chile*
[3]*Unité Mixte de Physique, CNRS, Thales, Université Paris-Saclay, 91767, Palaiseau, France*

(Received 11 May 2021; revised 15 July 2021; accepted 26 July 2021; published 4 August 2021)

Noncollinear chiral spin textures in ferromagnetic multilayers are at the forefront of recent research in nanomagnetism with the promise of fast and energy-efficient devices. The recently demonstrated possibilities to stabilize such chiral structures in synthetic antiferromagnets (SAFs) has raised interest as they are immune to dipolar field, hence favoring the stabilization of ultrasmall textures. They also improve mobility and avoid the transverse deflections of moving skyrmions limiting the efficiency in some foreseen applications. However, such systems with zero net magnetization are difficult to characterize by most of the standard techniques. Here, we report that the relevant parameters of a magnetic SAF texture, those being its period, its type (Néel or Bloch), and its chirality (clockwise or counterclockwise), can be directly determined using the circular dichroism in x-ray resonant scattering at half-integer multilayer Bragg peaks in reciprocal space. The analysis of the dependence in temperature down to 40 K allows us moreover to address the question of the temperature stability of a spin spiral in a SAF sample and of the temperature scaling of the symmetric and antisymmetric exchange interactions.

DOI: 10.1103/PhysRevB.104.L060402

In condensed matter, a large variety of physical phenomena hinge on the emergence of complex chiral windings of order parameters, their observation, and subsequently their control, especially in magnetism and spin-transport at the nanoscale. Spin-polarized scanning tunneling microscopy (SP-STM) revealed that magnetic textures with a cycloidal configuration of the magnetization and Néel domain walls are stabilized in ultrathin magnetic films (one or a few atomic layers) or heavy metal layers [1–3]. It was realized that these magnetic textures are in most cases stabilized by the interfacial Dzyaloshinskii-Moriya (DM) interaction in thin films [4,5], the antisymmetric analog of the Heisenberg interaction, favoring the twisting of neighboring spins around the DM vector. This interaction allows one to stabilize chiral domain walls or skyrmions, even at room temperature and with no applied magnetic field [6–8]. However, in ferromagnetic multilayers, even with only a few repetitions or in single films a few monolayers thick (and above), it has been shown that due to the presence of dipolar fields it is difficult to stabilize sub-100-nm-diam skyrmions [9,10] without external fields. In ferrimagnetic materials, the compensation of magnetic moments can significantly reduce this magnetic dipolar interaction, and indeed very recently such small magnetic skyrmions and chiral domains were reported in such systems [11–14]. A thermally more stable alternative to rare-earth ferrimagnetic systems is to rely on synthetic antiferromagnetic multilayers. In synthetic antiferromagnets (SAFs) it has been shown that spin spirals and skyrmions can be stabilized at room temperature [15] by a precise tuning of the effective perpendicular magnetic anisotropy (PMA), the DM interaction, and the Ruderman-Kittel-Kasuya-Yoshida (RKKY) [16] interlayer coupling.

In SAFs, the negligible stray field and zero total magnetization make them extremely challenging to investigate using techniques such as magnetic force microscopy (MFM), Lorentz transmission electron microscopy (TEM), or transmission geometry x-ray microscopy such as STXM or Ptychography. Only advanced MFM in vacuum or nitrogen-vacancy (NV) magnetometry permit clear imaging of such magnetic texture [15,17]. The need for a technique that allows one to probe chiral stability, 3D textures [18], or the ultrafast dynamics [19,20] of these magnetic textures is particularly crucial in the context of SAFs. Recently, we showed that the amplitude and sign of the circular dichroism in x-ray resonant magnetic scattering (XRMS) can determine the effective chirality, i.e., its type (Néel or Bloch) and its magnetic chirality in ferromagnetic multilayers (FMs) [21,22]. In the case of multilayers in which each magnetic layer is antiferromagnetically coupled to the next, a superlattice magnetic peak corresponding to twice the charge period Bragg peak is present in reflectivity when tuning the x-ray wavelength to a core-level edge of the magnetic material [23,24]. In this Letter, we show that by recording circular dichroism in XRMS at these positions in reciprocal space, we can directly access the chirality in SAFs hosting chiral spin spirals at remanance [15]. In addition, through temperature-dependent measurement we show that these spin spirals are stable with nearly constant period in the 40–300 K range. The constant period in this temperature range indicates that the ratio of the DM and exchange interaction amplitudes is temperature-independent.

TABLE I. Structure of SAF samples investigated. The description starts from the substrate side indicated by "//," thicknesses are given in nanometers in parentheses, and the numbers indexing the square brackets are the number of repetitions of the multilayer.

No.	Multilayer stack
I	//Pt(8)/[$Co_{0.4}Fe_{0.4}B_{0.2}$(0.9)/Ru(0.75)/Pt (0.5)]$_6$/Al(5)
II	//Pt(8)/[$Co_{0.4}Fe_{0.4}B_{0.2}$(0.9)/Ru(0.75)/Pt (0.5)]$_8$/Al(5)
III	//Pt(8)/[$Co_{0.4}Fe_{0.4}B_{0.2}$(0.9)/Ru(0.75)/Pt (0.5)]$_{10}$/Al(5)

The nominal stacking of the SAFs prepared by sputtering deposition is listed in Table I. They are Pt/CoFeB/Ru multilayers with three different numbers of repetitions, namely six, eight, and ten (see [15] for more details about the structures, the growth, and optimization). The XRMS experiments were performed using the RESOXS diffractometer [25] at the SEXTANTS beamline [26] of the synchrotron SOLEIL. They were conducted in reflectivity conditions for circularly left (CL) and right (CR) incident polarizations at the Fe L_3 edge (photon energy of 707 eV), with the diffracted x-rays collected using a standard Si photodiode or a Peltier-cooled square CCD detector covering 6.1 degrees at the working distance of 26 cm.

A typical $\theta/2\theta$ reflectivity, measured by photodiode, is displayed in Fig. 1(a) for sample II. The peak corresponding to the chemical modulation of the sample period of 2.15 nm is observed around a scattering angle of $\sim 26^\circ$ labeled as Q_{Bragg} [see the red arrow in Fig. 1(a)]. The first pure magnetic peak of the antiferromagnetic (AFM) ordering observed, for example, in Ag/Ni [23] or Co/Cu [24] similar antiferromagnetic multilayers is, however, not visible in our studied multilayers. The reason is that in the case of a perfectly AF coupled spin spiral with zero net magnetic moment in each layer, the pure magnetic specular reflection peak is not expected. In Fig. 1(b), we display the map of the intensity sum CL + CR and in Fig. 1(c) the difference CL − CR (bottom) for four incidence angles, two corresponding to the structural order at Q_{Bragg} and $2Q_{\mathrm{Bragg}}$ and two for the magnetic ordering at $Q_{\mathrm{Bragg}}/2$ and $3Q_{\mathrm{Bragg}}/2$. A diffraction ring is observed at particular angles, when the x-ray energy is tuned to the Fe L_3 edge. This ring

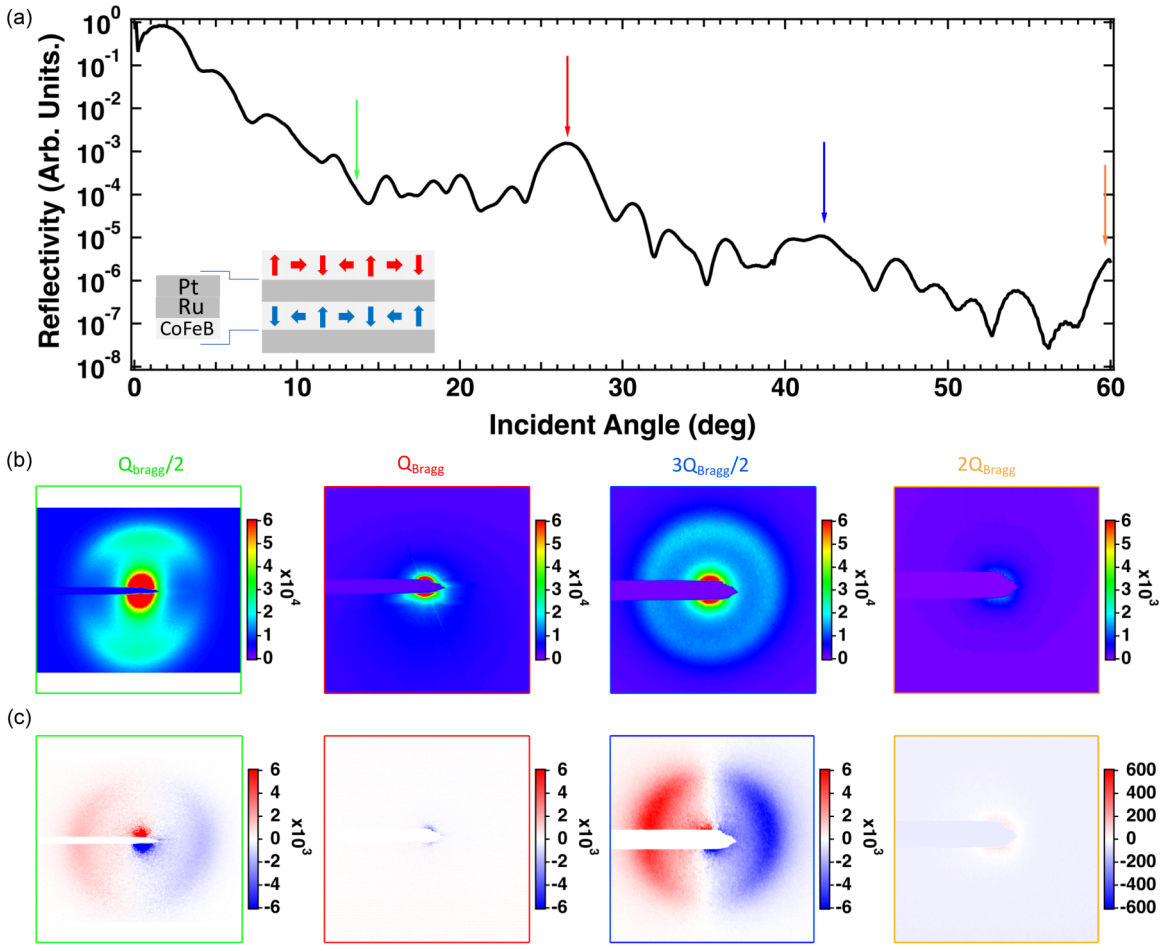

FIG. 1. (a) X-ray reflectivity recorded on sample III at 300 K and 707 eV using the sum (CL+CR) circularly polarized x-rays. The vertical red and orange arrows represent the position of the first- and second-order multilayer Bragg peaks arising from chemical periodicity. Green and blue arrows correspond to chemical half-Bragg peaks. (b) The sum image (CL + CR) using raw data (geometrically corrected to account for the projection related to the photon incidence angle) demonstrating more intense magnetic scattering at half Q_{Bragg} and an almost vanishing signal at Q_{Bragg}. (c) The difference image (CL − CR) using raw data showing intense (about 10% of the sum) magnetic asymmetry at $Q_{\mathrm{Bragg}}/2$ and almost vanishing magnetic asymmetry at Q_{Bragg} (see the text for details).

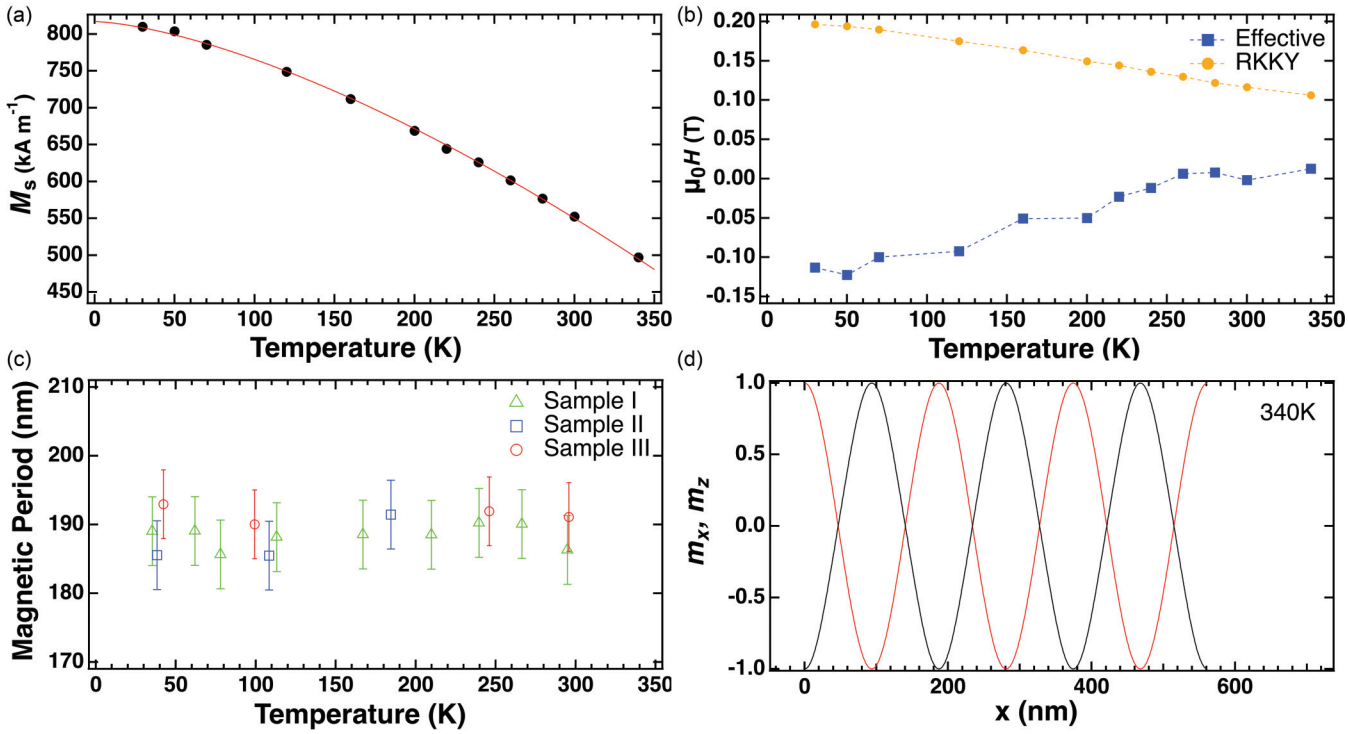

FIG. 2. (a) Temperature dependence of magnetization saturation for sample III. (b) Temperature dependance of $\mu_0 H_{\text{eff}}$ and $\mu_0 H_{\text{RKKY}}$ (lines are a guide to the eye) for sample III. (c) Temperature dependence of the magnetic period extracted from the XRMS pattern for all samples. (d) Horizontal and vertical components of the magnetization profile at 340 K obtained from micromagnetic simulations using the parameters displayed in (a)–(c).

reflects the labyrinthine spin spiral periodic magnetic texture of the sample which acts as a grating for x-rays. Because the magnetization in the two magnetic layers is coupled antiferromagnetically, the resonant magnetic scattering factors are reversed as well, resulting in the fact that x-ray scattering from successive planes will interfere destructively at the Bragg angle. This explains why we observe almost no diffraction ring either at Q_{Bragg} or at $2Q_{\text{Bragg}}$. On the contrary, at $Q_{\text{Bragg}}/2$ or at $3Q_{\text{Bragg}}/2$, the scattered light from layers having opposite magnetization will interfere constructively and give rise to intense diffraction rings. The reasoning on the experimental map of the intensity difference (CL − CR) shown in Fig. 1(c) is similar. The presence of a strong dichroic signal with a change of sign on either sides of the specular peak is a signature of the presence of a spin texture with a fixed chirality, as we demonstrated for FM multilayers [21,22]. Given the sign of the dichroic signal, we can compare it to our findings in previous studies [21,22] and conclude that counterclockwise (CCW) Néel magnetic textures are stabilized, as expected from the design of the multilayers with Pt underneath Co.

To analyze in more detail the intensity of the XRMS dichroism and later on its temperature dependence, we performed simulations of the XRMS signal using micromagnetic simulations as input. No modulation of the spin spiral along the z direction is obtained in the micromagnetic simulations performed at room temperature, indicating a negligible dipolar field contribution, with no 3D texture present, contrary to what was reported for a FM system [22]. Aiming to determine the spatial configuration of a spin-spiral order provided by the important magnetic parameters for the simulations, we measure the evolution of the saturation magnetization M_s as a function of temperature [see Fig. 2(a)] using a SQUID magnetometer. At room temperature, the saturation magnetization is 550 kA m^{-1}. We also measure the temperature dependence of $\mu_0 H_{\text{eff}}$ and $\mu_0 H_{\text{RKKY}}$, the effective PMA field and the RKKY coupling field, respectively [see Fig. 2(b)]. The magnetic period from the XRMS diffraction pattern is reported in Fig. 2(c). The trilayer repetition number (the sample) or the temperature are found not to change the period of the spin spiral, which takes a constant value of about 190 nm. As the spin spiral period, λ, is proportional to the ratio of the symmetric exchange stiffness A and the asymmetric (DM) one, D: $\lambda \approx 4\pi A/D$ [27–29], we can conclude that the ratio between these two parameters remains constant. To input realistic magnetization textures to the XRMS simulation program, we use MuMax3 [30] self-consistent solutions, minimizing the energy for the observed period, allowing us to estimate a consistent set of A and D parameters (see [15] for details). The results of the simulations are displayed in Fig. 2(d), in which the m_x and m_z components of the magnetization are plotted. Because D is large enough, ∼0.5 mJ m^{-2}, the m_y component of m is always zero. In the simulations, the spin spiral periodicity is found not to change for the three samples with different numbers of repetitions [see Fig. 2(c)], thus confirming the negligible dipolar field contribution in the SAF, unlike for FM multilayers [22].

Based on the results of the micromagnetic simulations, we now simulate the expected specular reflectivities and XRMS patterns and compare them with the experiments. While we have already simulated XRMS for FM multilayers assuming

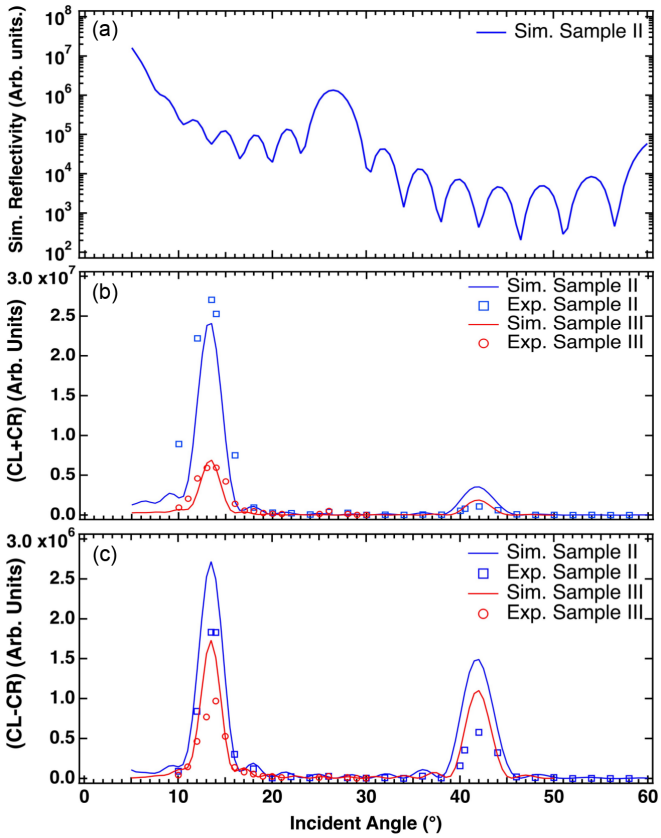

FIG. 3. (a) Simulation of reflectivity for sample II as a function of angle. (b) Simulations (lines) and experimental (dots) sum (CL + CR) as a function of incident angle for samples II (blue) and III (red). (c) Simulations (lines) and experimental sum (dots) (CL − CR) as a function of angle for samples II (blue) and III (red). Both simulation and experiment have been performed for an x-ray energy of 707 eV. (See the text for details.)

that all the magnetic layers have the same magnetization and considering only one layer [20,21], this is not a valid hypothesis in the case of AFM coupled multilayers. As a consequence, two layers have to be considered for the magnetic unit cell. Unlike for the hard-x-ray range, for which kinematic approximations can be used to simulate XRMS [31–34], simulation of resonant magnetic reflectivity requires dynamical approximation as the classical description with Maxwell equations and a permittivity built from the quantum scattering amplitude [35,36]. This approach has been successfully used in complex oxide heterostructures [37,38] demonstrating that the strong absorption and multiple scattering that become important especially at core-level resonance of $3d$ metals are well taken into account. Therefore, for this study we use the distorted wave born approximation (DWBA) to simulate XRMS [39–42], and we analyze the reflectivity simulated at the Fe L_3 edge (707 eV) for the sample II and III structure described in Table I. The simulated reflectivity curve in Fig. 3(a) exhibits a first and second Bragg peak, respectively, around ∼26° and ∼60°, similar to what was found in the experiment [Fig. 1(a)]. Even if we observe several differences, mainly because we used an idealized roughness-free sample in our simulation where only magnetic/nonmagnetic interfaces were considered, it does not alter the main point of this discussion. In Fig. 3(b), we display using open symbols the sum signal (CL+CR) angular dependence experimentally obtained by radial integration of the magnetic diffraction for both left and right circular polarization for samples II and III as well as the simulated ones using solid lines. CL and CR experimental intensities were plotted after removal of the diffuse background coming from the specular following the same approach previously used by Léveillé *et al.* [20].

We find in the simulated XRMS that the (CL + CR) intensity is almost vanishing at Q_{Bragg} and $2Q_{\mathrm{Bragg}}$ positions but is maximal at $Q_{\mathrm{Bragg}}/2$ and $3Q_{\mathrm{Bragg}}/2$. In Fig. 3(c), we plot the experimental dichroism (CL − CR) with symbols and the corresponding simulations with lines. For both samples and for (CL + CR) and (CL − CR) a very good agreement around $Q_{\mathrm{Bragg}}/2$ is found. For $3Q_{\mathrm{Bragg}}/2$ the simulations overestimate the sum and dichroism intensities. This difference can be explained by the fact that assuming an ideal structure for the simulation overestimates constructive interference at the Bragg angles. Again, the impact of the roughness of the multilayers is not taken into account in the simulations, which also leads to an overestimation of scattering intensity at high scattering angles. We would also like to point out that in order to have a better agreement at the $Q_{\mathrm{Bragg}}/2$ Bragg peak, a small variation in the spin spiral periodicity of 10 nm [remaining in the error bars from Fig. 2(c) in the x-y direction] has been included in the simulations. Note also that the dichroism is maximum at $Q_{\mathrm{Bragg}}/2$ and $3Q_{\mathrm{Bragg}}/2$ but remains nonzero for all angles and vanishes around Q_{Bragg}, $2Q_{\mathrm{Bragg}}/2$ and at grazing incidence. Experimental data for the six and ten repeat sample showed some weak magnetic signal between the half-Bragg angles, which was qualitatively reproduced in simulations by including some disorder along the z direction in the simulated multilayer.

We now turn to the temperature evolution of the magnetic asymmetry ratio, defined as $R = (\mathrm{CL} - \mathrm{CR})/(\mathrm{CL} + \mathrm{CR})$, measured at $Q_{\mathrm{Bragg}}/2$. To this end, we cooled the samples to 40 K (the lowest reachable temperature in the experiment) and measured the dichroism while gradually increasing the temperature. In Fig. 4, we see that despite the noticeable change of saturation magnetization, $\mu_0 H_{\mathrm{eff}}$ and $\mu_0 H_{\mathrm{RKKY}}$, the spin spiral state (period and chirality) is a metastable state that survives changes of the magnetic parameters over several tens of percent of relative variations. This demonstrates that the spin spiral state can be stabilized for a large range of magnetic parameters and that it is most probably possible to stabilize them for a rich variety of material compositions. Moreover, we have seen that the period of the spin-spiral order $4\pi A/D$ remains constant in the temperature range of 40–300 K, within which M_s varies by 30%. This provides strong evidence for one specific scenario of temperature scaling for the DM interaction. According to mean-field theory and its refinements, the symmetric (Heisenberg) exchange can be described by an amplitude A evolving with temperature as a function of M_s, following an $M_s(T)^{\sim 2}$ law, while M_s follows Bloch law $M_s(T) = M_s(0)[1 - (T/T_c)^{(3/2)}]$. We can thus deduce from the constant ratio A/D that D decreases with temperature following a similar $M_s(T)^{\sim 2}$ law, in agreement with other works [43].

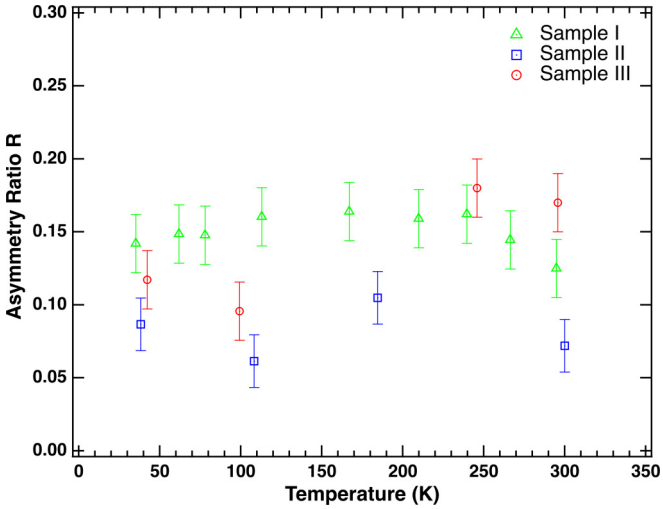

FIG. 4. Temperature dependence of the asymmetry ratio for sample I (red dots), sample II (green dots), and sample III (blue dots) measured at $Q_{\mathrm{Bragg}}/2$.

In summary, we report on the possibility of using circular dichroism in XRMS to determine the chiral properties of magnetic texture in SAF multilayers. We show experimentally that the magnetic diffraction and the difference between left and right circular polarization are maximal at positions in reciprocal space corresponding to the doubling of the chemical period, i.e., equal to the magnetic period in the sample. Our experimental findings have been confirmed by XRMS simulation using the DWBA with the results of micromagnetic simulations for input. We found an excellent agreement confirming our experimental result for both the diffracted intensity (CL + CR) and the dichroism (CL − CR). Finally, we also showed that independent of the number of periods, unlike for the FM multilayers, the period and the chirality of the spin spiral remain constant over a broad temperature range indicating a constant ratio A/D and thus their similar temperature scaling.

In a broader perspective, circular dichroism in x-ray scattering appears to be a unique tool to study chiral magnetic texture in SAF materials. We also would like to point out that this study opens the way for time-resolved studies of magnetic texture in AFM as it has recently been done for FM multilayers using the femtosecond x-rays pulses available at x-ray free-electron lasers (XFEL) [19,20] or high harmonic generation (HHG) sources [44,45].

Financial support from the Agence Nationale de la Recherche, France (ANR) with TOPSKY (ANR-17-CE24-0025), FLAG-ERA Sograph MEM (ANR-15-GRFL-0005, PCI2019-111908-2), and as part of the Investissements d'Avenir program SPiCY (ANR-10-LABX-0035), from Mineco grant AEI/FEDER, UE (FIS2016-7859-C3-2-R), and from the Horizon2020 Framework Program of the European Commission under FET-Proactive Grant SKYTOP (824123), is acknowledged.

[1] A. Kubetzka, M. Bode, O. Pietzsch, and R. Wiesendanger, Phys. Rev. Lett. **88**, 057201 (2002).
[2] E. Y. Vedmedenko, L. Udvardi, P. Weinberger, and R. Wiesendanger, Phys. Rev. B **75**, 104431 (2007).
[3] P. Ferriani, K. von Bergmann, E. Y. Vedmedenko, S. Heinze, M. Bode, M. Heide, G. Bihlmayer, S. Blügel, and R. Wiesendanger, Phys. Rev. Lett. **101**, 027201 (2008).
[4] A. Fert, Mater. Sci. Forum **59-60**, 439 (1990).
[5] M. Heide, G. Bihlmayer, and S. Blügel, Phys. Rev. B **78**, 140403(R) (2008).
[6] S. Woo, K. Litzius, B. Krüger, M.-Y. Im, L. Caretta, K. Richter, M. Mann, A. Krone, R. M. Reeve, M. Weigand, P. Agrawal, I. Lemesh, M-A. Mawass, P. Fischer, M. Kläui, and G. S. D. Beach, Nat. Mater. **15**, 501 (2016).
[7] C. Moreau-Luchaire, C. Moutafis, N. Reyren, J. Sampaio, C. A. F. Vaz, N. Van Horne, K. Bouzehouane, K. Garcia, C. Deranlot, P. Warnicke, P. Wohlhüter, J.-M. George, M. Weigand, J. Raabe, V. Cros, and A. Fert, Nat. Nanotechnol. **11**, 444 (2016).
[8] O. Boulle, J. Vogel, H. Yang, S. Pizzini, D. de Souza Chaves, A. Locatelli, T. Onur Menteß, A. Sala, L. D. Buda-Prejbeanu, O. Klein, M. Belmeguenai, Y. Roussigné, A. Stashkevich, S. M. Chérif, L. Aballe, M. Foerster, M. Chshiev, S. Auffret, I. Mihai Miron and G. Gaudin, Nat. Nanotechnol. **11**, 449 (2016).
[9] W. Legrand, N. Ronceray, N. Reyren, D. Maccariello, V. Cros, and A. Fert, Phys. Rev. Appl. **10**, 064042 (2018).
[10] F. Büttner, I. Lemesh, and G. S. D. Beach, Sci. Rep. **8**, 4464 (2018).
[11] L. Caretta, M. Mann, F. Büttner, K. Ueda, B. Pfau, C. M. Günther, P. Hessing, A. Churikova, C. Klose, M. Schneider, D. Engel, C. Marcus, D. Bono, K. Bagschik, S. Eisebitt, and G. S. D. Beach, Nature Nanotech. **13**, 1154 (2018).
[12] R. Streubel, C.-H. Lambert, N. Kent, P. Ercius, A. T. N'Diaye, C. Ophus, S. Salahuddin, and P. Fischer, Adv. Mater. **30**, 1800199 (2018).
[13] S. Woo, K. Mee Song, X. Zhang, Y. Zhou, M. Ezawa, X. Liu, S. Finizio, J. Raabe, N. Jong Lee, S.-I. Kim, S.-Y. Park, Y. Kim, J.-Y. Kim, D. Lee, O. Lee, J. Woo Choi, B.-C. Min, H. Cheol Koo, and J. Chang, Nat. Commun. **9**, 959 (2018).
[14] Y. Hirata, D.-H. Kim, S. Kwon Kim, D.-K. Lee, S.-H. Oh, D.-Y. Kim, T. Nishimura, T. Okuno, Y. Futakawa, H. Yoshikawa, A. Tsukamoto, Y. Tserkovnyak, Y. Shiota, T. Moriyama, S.-B. Choe, K.-J. Lee, and T. Ono, Nature Nanotech. **14**, 232 (2019).
[15] W. Legrand, D. Maccariello, F. Ajejas, S. Collin, A. Vecchiola, K. Bouzehouane, N. Reyren, V. Cros, and A. Fert, Nat. Mater. **19**, 34 (2020).
[16] S. S. P. Parkin, R. Bhadra, and K. P. Roche, Phys. Rev. Lett. **66**, 2152 (1991).
[17] A. Finco, A. Haykal, R. Tanos, F. Fabre, S. Chouaieb, W. Akhtar, I. Robert-Philip, W. Legrand, F. Ajejas, K. Bouzehouane, N. Reyren, T. Devolder, J-P. Adam, J-V. Kim, V. Cros, and V. Jacques, Nat. Commun. **12**, 767 (2021).

[18] E. Burgos, S. Flewett, Y. Sassi, W. Legrand, F. Ajejas, C. Léveillé, P. Gargiani, M. Valvidares, N. Reyren, V. Cros, and N. Jaouen (unpublished).
[19] N. Kerber, D. Ksenzov, F. Freimuth, F. Capotondi, E. Pedersoli, I. Lopez-Quintas, B. Seng, J. Cramer, K. Litzius, D. Lacour, H. Zabel, Y. Mokrousov, M. Kläui, and C. Gutt, Nat. Commun. **11**, 6304 (2020).
[20] C. Léveillé, E. Burgos-Parra, Y. Sassi, F. Ajejas, V. Chardonnet, E. Pedersoli, F. Capotondi, G. De Ninno, F. Maccherozzi, S. Dhesi, D. M. Burn, G. van der Laan, O. S. Latcham, A. V. Shytov, V. V. Kruglyak, E. Jal, V. Cros, J.-Y. Chauleau, N. Reyren, M. Viret, and N. Jaouen, arXiv:2007.08583.
[21] J.-Y. Chauleau, W. Legrand, N. Reyren, D. Maccariello, S. Collin, H. Popescu, K. Bouzehouane, V. Cros, N. Jaouen, and A. Fert, Phys. Rev. Lett. **120**, 037202 (2018).
[22] W. Legrand, J.-Y. Chauleau, D. Maccariello, N. Reyren, S. Collin, K. Bouzehouane, N. Jaouen, V. Cros, and A. Fert, Sci. Adv. **4**, eaat0415 (2018).
[23] J. M. Tonnerre, L. Sève, D. Raoux, G. Soullié, B. Rodmacq, and P. Wolfers, Phys. Rev. Lett. **75**, 740 (1995).
[24] C. Spezzani, P. Torelli, M. Sacchi, R. Delaunay, C. F. Hague, F. Salmassi, and E. M. Gullikson, Phys. Rev. B **66**, 052408 (2002).
[25] N. Jaouen, J.-M. Tonnerre, G. Kapoujian, P. Taunier, J.-P. Roux, D. Raoux, and F. Sirotti, J. Synch. Radiat. **11**, 353 (2004).
[26] M. Sacchi, N. Jaouen, H. Popescu, R. Gaudemer, J. M. Tonnerre, S. G. Chiuzbaian, C. F. Hague, A. Delmotte, J. M. Dubuisson, G. Cauchon, B. Lagarde, and F. Polack, J. Phys. Conf. Ser. **425**, 072018 (2013).
[27] C. Won, Y. Z. Wu, J. Choi, W. Kim, A. Scholl, A. Doran, T. Owens, J. Wu, X. F. Jin, and Z. Q. Qiu, Phys. Rev. B **71**, 224429 (2005).
[28] M. Bode, M. Heide, K. von Bergmann, P. Ferriani, S. Heinze, G. Bihlmayer, A. Kubetzka, O. Pietzsch, S. Blügel, and R. Wiesendanger, Nature **447**, 190 (2007).
[29] S. Meckler, N. Mikuszeit, A. Pressler, E. Y. Vedmedenko, O. Pietzsch, and R. Wiesendanger, Phys. Rev. Lett. **103**, 157201 (2009).
[30] A. Vansteenkiste, J. Leliaert, M. Dvornik, M. Helsen, F. Garcia-Sanchez, and B. Van Waeyenberge, AIP Adv. **4**, 107133 (2014).
[31] L. Sève, N. Jaouen, J. M. Tonnerre, D. Raoux, F. Bartolomé, M. Arend, W. Felsch, A. Rogalev, J. Goulon, C. Gautier, and J. F. Bérar, Phys. Rev. B **60**, 9662 (1999).
[32] N. Ishimatsu, H. Hashizume, S. Hamada, N. Hosoito, C. S. Nelson, C. T. Venkataraman, G. Srajer, and J. C. Lang, Phys. Rev. B **60**, 9596 (1999).
[33] N. Jaouen, J. M. Tonnerre, D. Raoux, E. Bontempi, L. Ortega, M. Müenzenberg, W. Felsch, A. Rogalev, H. A. Dürr, E. Dudzik, G. van der Laan, H. Maruyama, and M. Suzuki, Phys. Rev. B **66**, 134420 (2002).
[34] C. S. Nelson, G. Srajer, J. C. Lang, C. T. Venkataraman, S. K. Sinha, H. Hashizume, N. Ishimatsu, and N. Hosoito, Phys. Rev. B **60**, 12234 (1999).
[35] M. Elzo, E. Jal, O. Bunau, S. Grenier, A. Y. Ramos, H. Tolentino, Y. Joly, J.-M. Tonnerre, and N. Jaouen, J. Magn. Magn. Mater. **324**, 105 (2012).
[36] S. Macke and E. Goering, J. Phys. Condens. Matter **26**, 363201 (2014).
[37] M. Gibert, M. Viret, P. Zubko, N. Jaouen, J.-M. Tonnerre, A. Torres-Pardo, S. Catalano, A. Gloter, O. Stéphan, and J.-M. Triscone, Nat. Commun. **7**, 11227 (2016).
[38] G. Fabbris, N. Jaouen, D. Meyers, J. Feng, J. D. Hoffman, R. Sutarto, S. G. Chiuzbăian, A. Bhattacharya, and M. P. M. Dean, Phys. Rev. B **98**, 180401(R) (2018).
[39] D. R. Lee, S. K. Sinha, D. Haskel, Y. Choi, J. C. Lang, S. A. Stepanov, and G. Srajer, Phys. Rev. B **68**, 224409 (2003).
[40] D. R. Lee, S. K. Sinha, C. S. Nelson, J. C. Lang, C. T. Venkataraman, G. Srajer, and R. M. Osgood, Phys. Rev. B **68**, 224410 (2003).
[41] S. Flewett, T. J. A. Mori, A. Ovalle, S. Oyarzùn, A. Ibáñez, S. Michea, J. Escrig, and J. Denardin, Sci. Rep. **9**, 14823 (2019).
[42] S. Flewett, E. Burgos-Parra, M. Garrido Strelow, Y. Sassi, C. Léveillé, F. Ajejas, N. Reyren, and N. Jaouen, Phys. Rev. B **103**, 184401 (2021).
[43] Y. Zhou, R. Mansell, S. Valencia, F. Kronast, and S. van Dijken, Phys. Rev. B **101**, 054433 (2020).
[44] B. Vodungbo, J. Gautier, G. Lambert, A. B. Sardinha, M. Lozano, S. Sebban, M. Ducousso, W. Boutu, K. Li, B. Tudu, M. Tortarolo, R. Hawaldar, R. Delaunay, V. Lopez-Flores, J. Arabski, C. Boeglin, H. Merdji, P. Zeitoun, and J. Luning, Nat. Commun. **3**, 999 (2012).
[45] G. Fan, K. Legare, V. Cardin, X. Xie, E. Kaksis, G. Andriukaitis, A. Pugzlys, B. E. Schmidt, J. P. Wolf, M. Hehn, G. Malinowski, B. Vodungbo, E. Jal, J. Luning, N. Jaouen, Z. Tao, A. Baltuska, F. Legare, and T. Balciunas, arXiv:1910.14263 [physics.optics].